Second Quarterly Report | *Covering the Period 1 September to 30 November 1964*

THE DESIGN OF AN EXPERIMENT TO DETERMINE THE LIMITATIONS IMPOSED ON A MULTIPLE-APERTURE ANTENNA SYSTEM BY PROPAGATION PHENOMENA

By: J. H. BRYAN C. H. DAWSON F. G. FERNALD W. H. FOY, JR. J. PESCHON

Prepared for:

NATIONAL AERONAUTICS AND SPACE ADMINISTRATION
GODDARD SPACE FLIGHT CENTER
GREENBELT, MARYLAND

CONTRACT NAS 5-3974

STANFORD RESEARCH INSTITUTE

MENLO PARK, CALIFORNIA

*SRI

STANFORD RESEARCH INSTITUTE
MENLO PARK, CALIFORNIA

December 1964

Second Quarterly Report | *Covering the Period 1 September to 30 November 1964*

THE DESIGN OF AN EXPERIMENT TO DETERMINE THE LIMITATIONS IMPOSED ON A MULTIPLE-APERTURE ANTENNA SYSTEM BY PROPAGATION PHENOMENA

Prepared for:

NATIONAL AERONAUTICS AND SPACE ADMINISTRATION
GODDARD SPACE FLIGHT CENTER
GREENBELT, MARYLAND

CONTRACT NAS 5-3974

By: J. H. BRYAN C. H. DAWSON F. G. FERNALD W. H. FOY, JR. J. PESCHON

SRI Project 5067

Approved: DEAN F. BABCOCK, MANAGER
RADIO SYSTEMS LABORATORY

D. R. SCHEUCH, EXECUTIVE DIRECTOR
ELECTRONICS AND RADIO SCIENCES

Copy No. .....

ABSTRACT

19853

Work on the design of an experiment to determine propagation limitations on multiple-aperture antennas is reported for the period 1 September to 30 November 1964. This work has led to the following preliminary conclusions:

(1) The signal platform should be a satellite in a nonequatorial circular orbit with a period of more than 10 hours.

(2) Oscillator stability and transmitter power will not be limiting factors.

(3) A suitable beacon and/or transponder compatible with the NASA Minitrack or with established range, range-rate tracking systems should be provided. Angle data from NASA can be used for satellite acquisition.

(4) Kalman filtering techniques at the receiving site should be able to provide range-rate data to the required accuracy.

(5) The satellite should be able to transmit on any two of the frequencies 2, 4, 8, and 16 Gc simultaneously with coherent sidebands 100 or 200 Mc from each carrier.

(6) A minimum of five antennas each with amplitude monopulse feeds and three front ends should be provided. Four, of diameters 4, 8, 16, and 32 meters, can be fixed; one, of diameter 4 meters, must be moveable to separations of 1 km.

(7) A minimum of two receivers should be provided, each having a sum channel, two angle-error channels, and two sideband channels.

No final conclusions or recommendations can be reported at this time.

AUTHOR

CONTENTS

ILLUSTRATIONS

TABLES

I INTRODUCTION

This document reports on the work performed by SRI under Contract NAS5-3974 during the quarter ending 30 November 1964. This project, to design a space-to-earth propagation experiment, follows feasibility studies of multiaperture antenna systems by Electronic Communication, Inc., the Research Triangle Institute, and SRI. The experiment is to determine the limitations imposed by the propagation path on the multiaperture antenna.

The project consists of the following subtasks:

(1) System integration

(2) Signal sources

(3) Antenna drives

(4) Noise-correlation measurements

(5) Receivers

(6) Ionospheric measurements

(7) Meteorological measurements.

The work on each of the various subtasks is presented in Sect. II, except for Subtasks 4 and 6, which have not been active during the reporting period.

The system integration subtask is represented (in Sect. II-A) by a tentative description of the radio frequency equipment for the proposed experiments and an analysis of orbits and antennas leading to an estimate of satellite power. The signal source subtask is represented (in Sect. II-B) by an investigation of the possible use of the sun and radio stars as sources and of aircraft as signal platforms. The antenna drive subtask is represented (in Sect. II-C) by an analysis of the tracking system configuration, including error sources, and of signal source position prediction. The receiver subtask is represented (in Sect. II-D) by analyses of phase measurement including error sources and ambiguity resolution. The meteorological measurement subtask is represented (in Sect. II-E) by a preliminary report on the instrumentation and site-selection problems.

II DISCUSSION

A. SYSTEM INTEGRATION

1. RF EQUIPMENT

The following is a tentative description or listing of the RF equipment for the proposed experiment:

(1) A satellite-borne transmitter capable of transmitting by command, on carrier frequencies near 2, 4, 8, and 16 Gc should be used. Each carrier should have one or more coherent sidebands with 100 or 200 Mc separation giving a line spectrum; the multiple-frequency transmission will permit the separation of tropospheric and ionospheric effects and allow the determination of phase variations with frequency. The satellite should have a period of 10 hours or more to reduce Doppler effects and to allow taking of data over an essentially constant elevation angle for times of the order of a few minutes. The power must be sufficient to give S/N ratios near 20 db in a bandwidth of 100 cps.

(2) Five antennas should be provided: two 4-meter, one 8-meter, one 16-meter, and one 32-meter. All but one 4-meter antenna can have fixed and preferably adjacent locations. For space correlation studies, one 4-meter antenna should be moveable up to separations approaching one km. All antennas should have amplitude monopulse feeds and antenna-mounted front ends. Three, or possibly four, front ends will be required for each antenna: one or two for 2 and 4 Gc, one for 8 Gc, and one for 16 Gc.

(3) Two complete receivers should be available, each having a main channel, two angle-error channels, and one or more sideband channels.

(4) All antennas, including the moveable 4-meter dish, should be connected to the receiver building over lines whose delays can be measured; digital processing can be used later to determine the actual geometrical delay times. Conversely, the antenna-mounted front ends must be supplied from a master oscillator with equal, or at least measureable, phase shifts.

(5) Many recording channels will be required to include time as well as the receiver and tracking system outputs. Some outputs may be digital and should clearly be recorded

in digital form. For analog variables, the use of analog recording or quantization and digital recording is still to be determined.

2. Satellite Power

a. Geometry for Circular Orbits

An earth satellite in circular orbit has a period which satisfies

$$\frac{a^3}{T^2} = \frac{GM}{4\pi^2} \tag{1}$$

where $a = r + h$ = orbit radius in kilometers (km)

r = earth's radius = 6371 km

h = orbit height in km

T = orbital period in seconds (sec)

GM = constant = 3.986×10^5 $(\text{km})^3/(\text{sec})^2$.

The angular rate with respect to the center of the earth, ω_E, in radians per second (rad/sec) is

$$\omega_E = \frac{2\pi}{T} \quad . \tag{2}$$

The maximum angular rate with respect to a station on the surface of a nonrotating * earth, ω, occurs when the satellite is directly overhead and is given in rad/sec by

$$\omega = \frac{a}{h} \cdot \omega_E \quad . \tag{3}$$

The angle subtended by the earth at a satellite is

$$\theta = 2 \sin^{-1} \frac{r}{a} \tag{4}$$

and the range from the satellite to the horizon is

$$d = a \cos \frac{\theta}{2} \quad . \tag{5}$$

* The earth rotates at $2\pi/24 \cdot 60 \times 10^3 = 4.37$ milliradians/minute. Thus the maximum addition to the angular rate is $4.37\ a/h$ milliradians/minute.

When Eqs. (1) through (5) are applied to satellites with periods of 10, 17, and 24 hours, the results are as given in Table I.

Assuming that data runs do not exceed 5 minutes the elevation angle for any of the above orbits will vary by less than 0.0715 rad = 4.1° during a run. Hence the path conditions during the run can be considered constant.

Table I

GEOMETRICAL ORBIT QUANTITIES

T(hrs)	a(km)	h(km)	ω(mrad/min)	θ(rad)	d(km)
10	23,690	17,319	14.3	0.545	22,770
17	33,740	27,369	7.6	0.380	33,100
24	42,450	36,079	5.1	0.302	41,900

b. SPACE LOSS

The space loss between isotropic antennas is given by

$$L = (4\pi)^2 \frac{d^2}{\lambda^2} \tag{6}$$

where λ is the wavelength and d and λ are in the same units, However,

$$\lambda = \frac{c}{f \times 10^9} \tag{7}$$

where c is the velocity of propagation ($= 3 \cdot 10^5$ km/sec) and f is frequency in gigacycles (Gc).

Thus, substituting in Eqs. (7) and (6) with d in km,

$$L = (4\pi)^2 \frac{d^2 f^2 \times 10^{18}}{9 \times 10^{10}}$$

or in decibels (db)

$$L(\text{db}) = 20 \log \frac{4\pi}{3} \times 10^4 + 20 \log f + 20 \log d$$

$$= 92 + 20 \log f + 20 \log d. \tag{8}$$

For the altitudes in Table I and f = 2, 4, 8, and 16 Gc, the space loss is as given in Table II.

Table II

SPACE LOSS IN DB

T	FREQUENCY, Gc			
	2	4	8	16
10 hrs	185	191	197	203
17 hrs	188	194	200	207
24 hrs	190	196	203	209

c. GROUND ANTENNAS

For parabolic ground antennas with diameters D of 4, 8, 16, and 32 meters, the ratio $D/\lambda >> 1$ at frequencies of 2, 4, 8, and 16 Gc. Therefore, the following relations for half-power beamwidth θ_{HP}, and gain*, G, can be used:

$$G = \left(\frac{\pi D}{\lambda}\right)^2 \eta = 5.44 \left(\frac{D}{\lambda}\right) \tag{9}$$

$$\theta_{HP} = 1200 \left(\frac{\lambda}{D}\right) \tag{10}$$

where D and λ are in the same units, G is dimensionless, θ_{HP} is in milliradians (mrad), and η is efficiency, assumed to be 0.55. Substituting Eq. (7) in Eqs. (9) and (10) and expressing G in db gives

$$G(\text{db}) = 18 + 20 \log D + 20 \log f \tag{11}$$

$$\theta_{HP} = \frac{360}{fD} \text{ mrad} \tag{12}$$

where D is in meters and f in gigacyles.

The results for Eqs. (11) and (12) are given in Tables III and IV.

Table III

GROUND ANTENNA GAIN IN DB

DIAMETER METERS	FREQUENCY, Gc			
	2	4	8	16
4	36	42	48	54
8	42	48	54	60
16	48	54	60	66
32	54	60	66	72

Table IV

GROUND ANTENNA BEAMWIDTH, θ_{HP}, IN MILLIRADIANS

DIAMETER METERS	FREQUENCY, Gc			
	2	4	8	16
4	45	23	11	6
8	23	11	6	3
16	11	6	3	1
32	6	3	1	1

d. SPACE LOSS AND GROUND ANTENNA

When the antenna gain of Eq. (11) is combined with the space loss of Eq. (8), the net loss is

* These values assume no degradation due to surface or turbulence effects.

$$L - G = 74 + 20 \log d - 20 \log D \qquad (13)$$

which is independent of frequency.* The results are given in Table V.

Table V

NET LOSS IN DB

TIME	DIAMETER, METERS			
	4	8	16	32
10 hrs	149	143	137	131
17 hrs	152	146	140	134
24 hrs	154	148	142	136

e. RECEIVED SIGNAL POWER

The required receiver power, P_R, will be computed based on

T = system temperature = 600°K (System noise figure = 3.2 db)

B = information bandwidth = 100 cps

$2B$ = equivalent RF bandwidth = 200 cps

k = Boltzmann's constant = 1.38×10^{-23} joules/°K

S/N = 15 db.

Noise power = $P_N = kT[2B]$

$= 1.656 \times 10^{-18}$ watts

= −177 decibels with respect to 1 watt (dbw). (14)

Then

$$P_R = P_N + S/N = -162 \text{ dbw.} \qquad (15)$$

Table VI

EFFECTIVE TRANSMITTED POWER, P_E, IN DBW

TIME	DIAMETER, METERS			
	4	8	16	32
10 hrs	−13	−19	−25	−31
17 hrs	−10	−16	−22	−28
24 hrs	− 8	−14	−20	−26

f. EFFECTIVE TRANSMITTED POWERS

Combining Eq. (15) and Table V in the relation

Effective Transmitted Power = $P_E = P_R + L$ gives Table VI. (16)

g. SATELLITE ANTENNAS

If a single parabolic antenna were to be used for all four frequencies, its beam-width, and hence maximum diameter, would be set by the requirement that the whole earth be illuminated at the maximum frequency of 16 Gc. With such an antenna, and assuming the same aperture illumination, the gain would drop by 6 db for each octave decrease in frequency until the antenna

* Losses due to absorption and scattering have been neglected.

was no longer large in terms of wavelength and hence became equivalent to a dipole. An intermediate choice is to use two antennas, one for 2 and 4 Gc and one for 8 and 16 Gc. The extreme alternative, is to use a separate antenna for each frequency. There appear to be two possibilities, depending on whether (1) the satellite is completely stabilized with its axis pointing toward the earth, or (2) is spin stabilized with its axis perpendicular to the line joining the satellite and center of the earth.

If the satellite axis always points earthward, four parabolic antennas could be mounted with their apertures in a plane perpendicular to the axis. For this case Eqs. (11) and (12) again apply, using the subtended angle θ of Table I as the θ_{HP} of the antenna. The results are given in Tables VII and VIII. Note that the gain is independent of frequency. Since the horizon is at the half-power angle, the horizon gain is down by a factor of 2.

Table VII

SATELLITE ANTENNA DIAMETERS
(D in centimeters)

T	FREQUENCY, Gc			
	2	4	8	16
10 hrs	33	17	8	4
17 hrs	47	24	12	6
24 hrs	60	30	15	7

Table VIII

GAIN VALUES FOR SATELLITE PARABOLIC ANTENNAS

T(hrs)	MAXIMUM GAIN (db)	HORIZON GAIN (db)
10	14	11
17	17	14
24	20	17

The effect of spinning these antennas has not been investigated.

It might also be possible to design a nested set of Cassegrain parabolic antennas, where the back of each dish provided the reflector for the antenna of the next lower frequency. However, aperture blockage would be severe.

If the satellite axis is perpendicular to a radial line from the center of the earth, then an antenna whose pattern is symmetrical about the spin axis and whose maximum gain is perpendicular to its axis is required. The half-wave dipole fulfills these requirements with a maximum gain of 2.1 db and a half-power beamwidth of 1.361 radians. The relative power at an angle α from the axis is given by

$$G_R = \left[\frac{\cos(\pi/2 \cos \alpha)}{\sin \alpha}\right]^2 . \qquad (17)$$

Here, α is related to the subtended beamwidth by

$$\alpha = \frac{1}{2}[\pi - \theta] \quad . \tag{18}$$

When the values of θ from Table I are used in Eqs. (18) and (19), the relative and net gains of the dipoles are as given in Table IX.

Such a set of dipole antennas might be constructed as a series of cylinders extending from the satellite along its spin axis. The 2-Gc dipole would be next to the satellite and would include a coaxial feed for the other antennas. Other possibilities are a biconical horn and a log periodic antenna.

Table IX

GAIN VALUES FOR SATELLITE DIPOLE ANTENNAS

T(hrs)	G_R(db)	MAXIMUM GAIN (db)	HORIZON GAIN (db)
10	-0.5	2.1	1.6
17	-0.2	2.1	1.9
24	-0.2	2.1	1.9

h. TRANSMITTED POWER

Since the effective transmitted power, P_E, is equal to the product of the transmitter antenna gain at the horizon and the transmitter power, P_T,

$$P_T(\text{dbw}) = P_E(\text{dbw}) - G(\text{db}) \quad . \tag{19}$$

Table X

MINIMUM SATELLITE TRANSMITTER POWER, P_T, IN DBW

T(hrs)	PARABOLIC*	DIPOLE
10	-24	-15
17	-24	-12
24	-25	-10

For the case involving parabolic satellite antennas, operation at the horizon, and a 4-meter receiving antenna, the minimum transmitter power (from Tables VI and VIII) is as given in Table X. When dipole satellite antennas are used, the minimum transmitter power (from Tables VI and IX) is also as given in Table X.

Since a transmitted power of 1 watt (0 dbw) is entirely practical, the powers in Table X indicate considerable margin even when several tones are transmitted simultaneously.

* Note that the required transmitted power is essentially independent of satellite height; the increased space loss at the greater heights is almost matched by the increased satellite antenna gain due to a smaller subtended angle.

B. SIGNAL SOURCES

During the past quarter, information has been sought about the possible use of the sun and the radio stars as signal sources for estimating the decorrelation of microwave-signal phase fluctuations across the plane of an array of receiving antennas. The sun is by far the strongest natural radio source, but its relatively wide angular extent suggests that its radio signals, even in the absence of a troposphere, might be phase-correlated at the earth's surface over relatively short distances only. Available reference material has yielded evidence that this kind of effect has been a matter of concern for some workers:[1*]

> Interferometers of (the) twin-wave type have been commonly used for the identification of small sources of radio waves, *e.g.*, radio stars or sources of small area on the sun, and for the location and measurement of the size of such sources .... They suffer from a very serious limitation, however, in that records obtained from them are very difficult to interpret whenever two or more point sources are simultaneously present in the beam of the primary aerials or the source is extended.

It would be difficult in experimental work to resolve the phase differences at separated antennas resulting from atmospheric propagation effects from those attributable to the extended source itself; in two reports of experimental work[2,3] no effort to resolve such effects is indicated in comparisons of amplitude scintillation of solar microwave radiation received at spaced antennas. As suggested above, and as evident in measurements reported in Ref. 2 and in the "Solar-Geophysical Data" published by the National Bureau of Standards,[4] the sun at microwave frequencies can appear to be a very non-uniform source of radiant energy, with strong small-area sources scattered over its surface. The strength of over-all radiation from the sun, moreover, varies over about an order of magnitude from average "quiet sun" conditions to "flare-and-burst" conditions at 3 cm, and over about two orders of magnitude at 30 cm. If such flare-and-burst activity were confined to small regions of the sun, yielding effectively point sources from one to two orders of magnitude brighter than the rest of the sun, and if such activity occurred fairly often and for useful durations, these might serve as usable signal sources for estimated atmospheric decorrelation of signals across an antenna array.

---

* References are listed at the end of the report.

The required order of stability of the effective center of radiation on the sun, relative to the sun's diameter, can be estimated as follows: In order to get useful information about decorrelation over the earth's surface of atmospheric phase perturbations, the antennas must be separable by at least a distance of the order of 100 meters. At this distance, and at the lowest frequency of concern (1 Gc), the magnitude (rms) of tropospheric fluctuations of phase is expected from previous observations[8] to be of the order of 0.1 radian or less. Hence, if the fluctuations were uncorrelated at the two antennas, the difference-signal phase fluctuation would be of this order. This is equivalent to a random fluctuation of the angular position of a point source of radiation of the order of 10^{-5} radian in the sky, or about 1/1000 of the sun's diameter. If the effects of random wander of the sun's effective center of radiation are to be an order of magnitude smaller than the atmospheric effects of concern here, the wander then must be no greater than about 1/10,000 of the sun's diameter. It is not known whether stability of this kind in the sun's effective center of radiation is maintained for intervals long enough to be useful for making observations of atmospheric effects—*i.e.*, for intervals of the order of seconds to minutes. The angular resolution of solar spectroheliograms measured at Stanford University is about 10^{-3} radians. A cursory examination of some of these spectroheliograms indicates that in the recent past, regions of strong radiation have diameters of the order of 1/6 of the sun's diameter, and their contribution to the total solar flux at 9.1 cm is only of the order of 10%. Use of the sun as reference therefore does not seem promising, but there appear to be some inconsistencies or gaps in our present picture of the solar radiation.

At Stanford, two 30-foot dishes that can be moved have been used for observing radio stars at various distances on *N-S* baselines. No details have been obtained as yet on their operation, but they are reported to be measuring scintillations that may be attributable to atmospheric effects. Calculations of available flux density from the brightest radio stars in the range from 1 to 10 Gc suggest that very large dishes would be needed to measure the decorrelation of tropospheric phase perturbations along the earth's surface even with a low-noise receiver, and it is of interest to determine just what system is in use at Stanford. Reference 3 discusses the measurement of amplitude scintillation of radio star radiation at 1200 and 2980 Mc to observe gross tropospheric effects, and includes this brief but interesting summary (unfortunately no details of measurement are included):

The atmospheric scintillations in the upper microwave region have peaks several times the mean values of the source. The correlation between peaks and nulls at 1200 and 2980 Mc ranged from 0.4 to 0.7, indicating weak frequency dependence of the scintillation mechanism. Analysis of Cygnus *A* risings and settings during the period 1961-1962 shows that the mean rate of fluctuation increases as elevation angle increases, while the mean index decreases sharply. The day-to-day variations are considerable but show no correlation with obvious gross weather characteristics.

An effort has been made to estimate the possible usefulness of aircraft or balloons as high-altitude transmitter platforms for experimental work. The high speed of aircraft motion and consequent rapid scanning of the line of sight through the tropospheric irregularities would distort the spectral distribution of the phase fluctuations, and would have to be taken out in processing the data, to the extent that the trajectory and speed of the aircraft were known. Irregular motions of the aircraft would also introduce uncertainty into estimates of the magnitudes of the phase fluctuations produced by the troposphere. Cornell Aeronautical Laboratory (CAL) has made a series of measurements of this kind using *S*-band signals, and H. A. von Biel has published some preliminary results in Ref. 5. By using an interferometer receiving system, the measurement scheme used by CAL greatly reduces the phase errors attending irregular platform motion. It also reduces considerably the stability requirement on the system transmitter. (From the parameters of the CAL measurement arrangement, it appears that a stability of 1 part in 10^7 would be adequate to keep resulting errors about an order of magnitude lower than the magnitudes being measured.) If the elements of the interferometer are widely spaced, compared with a characteristic dimension of a tropospheric inhomogeneity ("blob"), the propagation paths to the two elements can be considered to produce independent phase fluctuation on the signals to these elements over much or perhaps most of the path length. The uncertainties associated with this independence are the price paid for the reduction in the errors that are produced by unmeasured or erratic platform motion and by transmitter instability. Further investigation may confirm the apparent advantages of interferometer measurement methods; it may also show up further shortcomings of the use of an aircraft platform, shortcomings that might be aggravated or ameliorated by placing the transmitter on a balloon platform or on a satellite.

C. ANTENNA DRIVES

The angle-of-arrival fluctuations $\Delta\theta$ and $\Delta\psi$ associated with the azimuth and elevation axes θ and ψ are determined by pointing the antenna into the geometrical direction of the signal source. The amplitude monopulse receivers (one for azimuth and one for elevation) then measure the fluctuation $\Delta\theta$ and $\Delta\psi$.

These fluctuation measurements are affected by some or all of the following errors, depending on the tracking system used:

(1) Error in predicting the signal-source location

(2) Gravity-, thermal-, and wind-induced pointing errors

(3) Transient and read-out errors

(4) Receiver noise in the error channel.

1. Open-Loop Tracking

The open-loop tracking system consists of the antenna whose servo is commanded by the target position data received from the NASA tracking network. Since these position data do not correspond to the local coordinates and are not received sufficiently often, coordinate conversion and interpolation must be performed by a local digital computer, such as that developed by JPL.

All the above-listed errors are present in the open-loop tracking system. No separation of signal from noise is possible since the errors are all located in the frequency spectrum of the signal, which extends from 0 to probably over 100 cps. The measurement of the very low frequencies ($f < 0.01$ cps) of the fluctuation spectrum will be heavily contaminated by bias errors in signal source position prediction and gravity effects as well as thermal-induced errors. Wind-induced errors predominate at somewhat higher frequencies ($0.1 < f < 1$ cps) whereas receiver noise is present throughout the whole frequency band to be observed.

It is felt at this time that, even though the very low frequencies in the $\Delta\theta$ and $\Delta\psi$ spectra can in principle be measured by open-loop tracking, the accuracies will be intolerably low. The constant bending of optical rays as a function of elevation is well known, and, furthermore, this bending does not affect adversely the performance of an antenna controlled by its own (local) tracking system.

2. Closed-Loop Tracking

The closed-loop tracking system consists of the antenna whose servo is commanded by the predicted target position $\hat{x}$, as well as by a correcting signal θ^* supplied by the filter F connected to the tracking receivers (amplitude monopulse). This is shown in the block diagram of Fig. 1 for one axis.

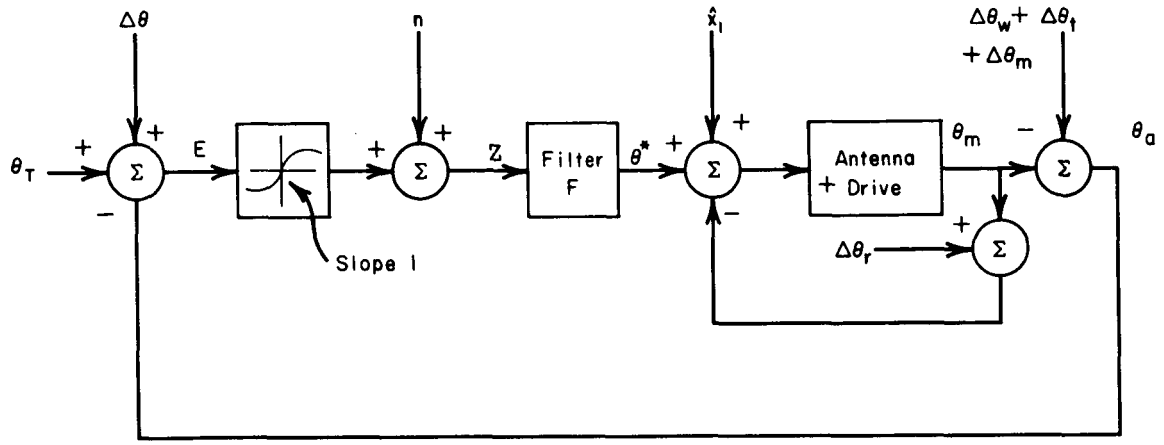

θ_T = True target positon excluding constant atmospheric bending

$\hat{x}_1$ = Predicted target position including constant atmospheric bending

$\Delta\theta$ = Bending angle of the propagation path

Z = Output of monopulse difference channel

θ_m = Position of mechanical antenna axis

θ_a = Position of electrical antenna axis

$\Delta\theta_w$ = Wind induced error occurring outside the servo loop

$\Delta\theta_f$ = Thermal induced error

$\Delta\theta_m$ = Gravity induced error

n = Receiver noise

$\Delta\theta_r$ = Readout error

$\Delta\theta_T = \theta_T - \hat{x}_1$ = error in predicting target position

TA-5067-1

FIG. 1 CLOSED-LOOP SYSTEM

This tracking system differs from most conventional tracking systems in that the servo loop remains closed and that the predicted target motion $\hat{x}_1$ is used as a command input to the servo system. The purpose of this is to reduce wind-induced errors occurring *inside* the servo loop as well as tracking errors caused by a nonstationary signal source. For further details, see Ref. 6.

If the filter F had a very long dominant time constant $\tau(\tau = 1/2\pi f >> 1/2\pi)$, then the errors $\Delta\theta_w$, $\Delta\theta_t$, $\Delta\theta_m$, n, the signal $\Delta\theta$, and the tracking error $\Delta\theta_T$ would all appear at the summing node Z, except for the very low frequency components of $\Delta\theta_w$, $\Delta\theta_t$, $\Delta\theta_m$, n, $\Delta\theta$ and $\Delta\theta_T$. It can indeed be shown that*

$$Z(s) \approx \frac{\Delta\theta_T + n + \Delta\theta + \Delta\theta_w + \Delta\theta_t + \Delta\theta_m - \Delta\theta_r}{1 + F(s)} \tag{20}$$

$$Z(s) = \mathcal{L}[z(t)] \quad .$$

In order to ensure steady-state accuracy, the filter $F(s)$ contains at least one integration, *i.e.*,

$$F(s) = \frac{N(s)}{sD(s)} \quad . \tag{21}$$

Hence, for $s \to 0$, $Z(s) \to 0$; the significance of this result is that the very low frequency components of any of the numerator variables in Eq. (20) are lost.

For $s = jw$, $w \neq 0$, the response $Z(jw)$ to any of the numerator variables, for example $\Delta\theta(jw)$ is

$$Z(jw) = \frac{\Delta\theta(jw)}{1 + F(jw)} \quad . \tag{22}$$

Consequently, if the filter transfer function is designed such that

$$F(jw) \to 0 \qquad \text{for } w > w_0 \tag{23}$$

then all the frequency components above w_0 of the numerator variables in Eq. (20) are included in $Z(jw)$.

---

* With reference to Fig. 1, we may write:

$$Z = n + \theta_T - \theta_a + \Delta\theta$$

$$\theta_a = \theta_m - \Delta\theta_w - \Delta\theta_t - \Delta\theta_m$$

If $G(s)$ is the transfer function of the antenna and its drive, then

$$\theta_m = (\vartheta^* + \hat{x}_1 + \Delta\theta_r)\{G(s)/[1 + G(s)]\} \quad .$$

Relating θ^* to Z by $\theta^*(s) = F(s)Z(s)$, and combining the above equations, it follows that

$$Z(s) = \frac{(n + \theta_T + \Delta\theta + \Delta\theta_w + \Delta\theta_t + \Delta\theta_m) - (\hat{x}_1 + \Delta\theta_r)[G/(1 + G)]}{1 + [FG/(1 + G)]} \quad .$$

For signals varying at a rate of less than 1 cps, $G/(1 + G)$ is very nearly equal to unity for most high-performance antenna drives. Under this assumption, $Z(s)$ simplifies to the expression in Eq. (20).

The thermal- and gravity-induced perturbations, $\Delta\theta_t$ and $\Delta\theta_m$, vary very slowly with time and therefore do not contribute to the measurement Z.

The other perturbations, *i.e.*, $\Delta\theta_T$, n, $\Delta\theta_w$, and $\Delta\theta_r$, have higher frequency components and hence do contribute to the measurement Z. It is therefore essential that the amplitude of these perturbations be kept to a minimum; this involves an accurate predictor of the motion θ_T, a high quality servo system to minimize $\Delta\theta_r$, a radome to eliminate $\Delta\theta_w$ and a sufficiently powerful signal source to provide a high S/N ratio at the output of the monopulse difference channel.

3. The Target Position Predictor

The motion $\hat{x}(t)$ of passive space vehicles, such as those considered here to carry the signal source, obey known equations with comparatively small perturbation terms. Consequently, if at any time t_0, the position vector $\hat{x}_1(t_0)$ and velocity vector $x_2(t_0) = dx_1/dt$ are known, the motion for all later times can be obtained with good accuracy by integration of the equations of motion.

If the position and velocity measurements are corrupted by noise, it is still possible to estimate the true target motion with quite small error, provided that the noisy measurement is performed over a sufficiently long period of time.

The filter which provides the optimum (in the least-squares sense) estimate $\hat{x}_1(t)$ and $\hat{x}_2(t)$ of target position and velocity was developed several years ago by Kalman and Bucy,[7] and will, in what follows, be referred to as the Kalman filter.

In order to illustrate the characteristics of this filter, we assume that

(1) Target motion is restricted to one axis (elevation)

(2) Target motion is of the form $x_1(t) = a_0 + a_1 t$

(3) The constants a_0 and a_1 are unknown

(4) The measurement $y(t)$ is $x(t) + N(t)$, where $N(t)$ is the measurement noise

(5) The measurement noise $N(t)$ is white, Gaussian, of variance $\sigma_N^2(t)$. (24)

The motion $x_1(t)$—see Eq. 24—is represented by the differential equations

$$\begin{aligned} \dot{x}_1(t) &= x_2(t) & x_1(0) &= a_0 \\ \dot{x}_2(t) &= 0 & x_2(0) &= a_1 \quad . \end{aligned} \tag{25}$$

Equation (25) is usually written as a matrix differential equation

$$\dot{\underline{x}} = F\underline{x} \tag{26}$$

with

$$\underline{x} = \begin{bmatrix} x_1 \\ x_2 \end{bmatrix} \qquad F = \begin{bmatrix} 0 & 1 \\ 0 & 0 \end{bmatrix} \quad .$$

The measurement y—here the elevation angle—is related to $\underline{x}$ by the equation

$$y = H\underline{x} + N \tag{27}$$

with

$$H = [1 \quad 0] \quad .$$

The output of the Kalman filter is a vector $\hat{\underline{x}}$, the components $\hat{x}_1(t)$ and $\hat{x}_2(t)$ of which are the current best—in the least squares sense—estimates of $\underline{x}(t)$. We define the variance matrix $P(t)$

$$P(t) = \begin{bmatrix} p_{11}(t) & p_{12}(t) \\ p_{12}(t) & p_{22}(t) \end{bmatrix} \tag{28}$$

the elements of which are*

$$\begin{aligned} p_{11}(t) &= < [x_1(t) - \hat{x}_1(t)]^2 > \\ p_{22}(t) &= < [x_2(t) - \hat{x}_2(t)]^2 > \\ p_{12}(t) &= < [x_1(t) - \hat{x}_1(t)][x_2(t) - \hat{x}_2(t)] > \quad . \end{aligned}$$

Kalman's filter reduces the variance matrix P in accordance with the so-called matrix variance equation

* The symbol $< >$ denotes an ensemble average.

$$\dot{P} = FP + PF^T - \frac{1}{\sigma_N^2} PH^T HP \qquad (29)$$

the steady-state solution of which is $P = 0$, *i.e.*, zero error in the estimate of x.

The filter is described by

$$\dot{\hat{\underline{x}}} = F\hat{\underline{x}} + K(y - H\hat{\underline{x}}) \quad . \qquad (30)$$

Its structure is shown in Fig. 2.

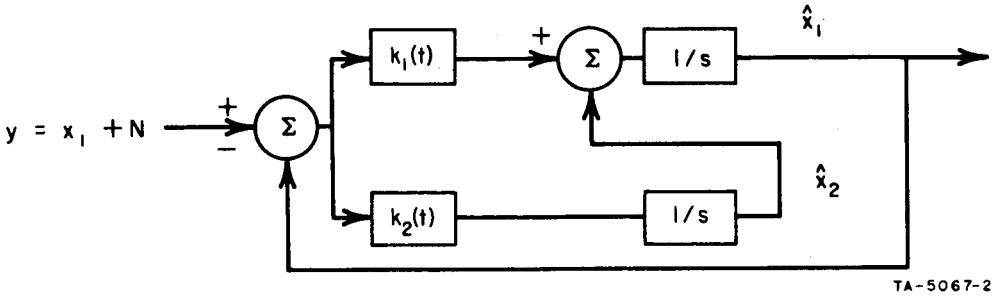

FIG. 2 KALMAN FILTER

The variable gains k_1 and k_2 are given by the vector equation

$$K(t) = \begin{bmatrix} k_1(t) \\ k_2(t) \end{bmatrix} = \frac{1}{\sigma_N^2} PH^T \quad . \qquad (31)$$

It should be noted that the "time constant" of the Kalman filter* increases as time proceeds, since $K(t) \to 0$ for $t \to \infty$. This "time-constant" is indeed

$$\frac{2}{k_1(t)} \quad .$$

Since y is not directly measurable on the monopulse difference channel, it will be synthesized as shown in Fig. 3.

* To be rigorous, a time constant should only be associated with a 1^n-order stationary linear system. It is, however, convenient and customary to define a time constant for other systems, such as the nonstationary system under discussion.

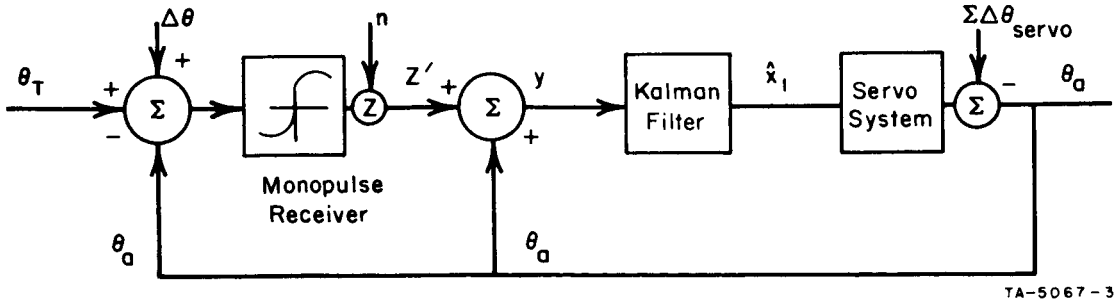

FIG. 3 KALMAN TRACKING LOOP

4. Over-All System

Instead of using separate filters to provide the signal $Z(t)$—see Fig. 1—and the predicted motion $\hat{x}_1(t)$, it is possible to use the Kalman filter to accomplish both filtering tasks. The signal Z' of Fig. 3 is indeed identical to the signal Z of Fig. 1; the stationary filter $F(s)$ is replaced by the time-varying Kalman filter which has an extremely long time constant and, therefore, allows a measurement of $\Delta\theta$ down to almost zero frequency. Since target prediction errors $\Delta\theta_T$ are virtually eliminated, the major remaining error source is $\Sigma\Delta\theta_{servo}$; that is, all the non-dc servo errors, of which wind-induced errors are probably predominant.

5. Computational Requirements

As evidenced by Eqs. (10), (11), and (12), implementation of the Kalman filter involves a real-time digital computer. It appears that a small machine, already required for other local computational tasks, will suffice. If a more complete analysis of the Kalman filter leads to unacceptable computational requirements, the nonoptimal time-varying filter discussed in Ref. 1 will be synthesized instead. The latter filter is very economical in terms of computational requirements.

D. RECEIVERS

1. Measurement of Path-Length Variations

The electromagnetic propagation path from a spacecraft to the earth has an electrical length which differs from its geometrical length. This increase in length is due to the decreased velocity of propagation in blobs

existing in the troposphere and the ionosphere. These length variations may be studied by receiving sinusoidal signals transmitted from a spacecraft oscillator. The resulting received signals will, of course, not be truly sinusoidal; however, the processes which modify the signals have bandwidths which are very much smaller than the carrier frequencies of interest. The received signals can therefore be considered as sinusoids of slowly varying frequency and phase.

The spacecraft oscillator will have an output frequency $\omega_2(t)$ which will consist of three components:

(a) ω_0, the average frequency over the period of interest (ω_0 is assumed to be accurately known at the receiver)

(b) $\omega_1(t)$, the slowly varying component of frequency (ω_1 can be called frequency noise and is due to temperature, power supply, and component changes)

(c) $\dot{\theta}_0(t)$*, the frequency component due to phase jitter, $\theta_0(t)$, in the oscillator and transmitter.

Thus, the transmitted frequency is

$$\omega_2(t) = \omega_0 + \omega_1(t) + \dot{\theta}_0(t) \quad . \tag{32}$$

Since both $\omega_1(t)$ and $\theta(t)$ can be assumed to be stationary processes, their statistics, and hence those of $\omega_2(t)$, are independent of the propagation delay between the transmitter and the receiver.

The propagation path will have an electrical path length of $p(t)$ which consists of two components:

(1) $r(t)$, the geometric path length including refraction effects

(2) $d(t)$, the increase in path length due to path inhomogeneities.

Thus

$$p(t) = r(t) + d(t) \tag{33}$$

and

$$\dot{p}(t) = \dot{r}(t) + \dot{d}(t) \quad . \tag{34}$$

Applying the usual nonrelativistic Doppler relation, the received frequency, $\omega_3(t)$, is

* The super dot denotes differentiation with respect to time.

$$\omega_3(t) = \omega_2(t)\left[1 - \frac{\dot{p}(t)}{c}\right] \tag{35}$$

where c is the velocity of light.

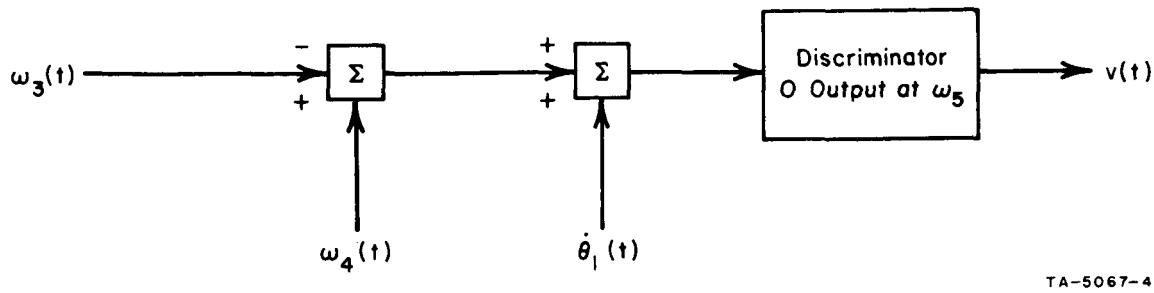

FIG. 4 RECEIVER STRUCTURE (Frequency)

Consider the receiver structure of Fig. 4, where $\omega_4(t)$ is the output of a local oscillator nominally ω_5 radians/second above the received frequency $\omega_3(t)$. The difference signal frequency, $\omega_4(t) - \omega_3(t)$, plus the frequency component, $\dot{\theta}_1(t)$, due to receiver phase jitter, is fed to a frequency discriminator whose output, $v(t)$, is proportional to frequency

$$v(t) = [\omega_4(t) - \omega_3(t) + \dot{\theta}_1(t)] - \omega_5 \quad . \tag{36}$$

The receiver also makes estimates of $\omega_1(t)$ and $\dot{r}(t)$:

$$\hat{\omega}_1(t) = \omega_1(t) + \Delta_0(t) \tag{37}$$

$$\hat{\dot{r}}(t) = \dot{r}(t) - \Delta_1(t) \tag{38}$$

where Δ_0 and Δ_1 are the estimation errors. The local oscillator frequency is synthesized as

$$\omega_4(t) = [\omega_0 + \hat{\omega}_1(t)]\left[1 - \frac{\hat{\dot{r}}(t)}{c}\right] + \omega_5$$

$$= [\omega_0 + \omega_1(t) + \Delta_0(t)]\left[1 - \frac{\dot{r}(t) - \Delta_1(t)}{c}\right] + \omega_5 \quad . \tag{39}$$

When Eqs. (32), (34), (35) and (39) are substituted in Eq. (36)

$$v(t) = [\omega_0 + \omega_1(t) + \Delta_0(t)]\left[1 - \frac{\dot{r}(t) - \Delta_1(t)}{c}\right] + \omega_5$$

$$- [\omega_0 + \omega_1(t) + \dot{\theta}_0(t)]\left[1 - \frac{\dot{r}(t) + \dot{d}(t)}{c}\right] + \dot{\theta}_1(t) - \omega_5 \quad . \qquad (40)$$

After expansion and simplification, Eq. (40) becomes

$$v(t) = \left[\frac{\omega_0}{c}\dot{d}(t) + \Delta_0(t) + \frac{\omega_0}{c}\Delta_1(t) - \dot{\theta}_0(t) + \dot{\theta}_1(t)\right]$$

$$+ \frac{1}{c}[\omega_1(t)\Delta_1(t) - \Delta_0(t)\dot{r}(t) + \Delta_0(t)\Delta_1(t) + \dot{\theta}_0(t)\dot{r}(t)$$

$$+ \omega_1(t)\dot{d}(t) + \dot{\theta}_0\dot{d}] \quad . \qquad (41)$$

Making the reasonable assumption that ω_1, Δ_1, Δ_0 and $\dot{r}/c$, are small quantities, all of the second set of terms in Eq. (41) can be neglected. Thus $v(t)$ is given approximately by:

$$v(t) = \frac{\omega_0}{c}\dot{d}(t) + \Delta_0(t) + \frac{\omega_0}{c}\Delta_1(t) + \dot{\theta}_2(t) \qquad (42)$$

where

$$\dot{\theta}_2(t) = \dot{\theta}_0(t) + \dot{\theta}_1(t) \quad . \qquad (43)$$

Solving Eq. (43) for $\dot{d}(t)$, the quantity to be measured, there results

$$\dot{d}(t) = \frac{c}{\omega_0}v(t) - \left[\frac{c}{\omega_0}\Delta_0(t) + \Delta_1(t) + \frac{c}{\omega_0}\dot{\theta}_2(t)\right] \qquad (44)$$

where $(c/\omega_0)v(t)$ must be taken as the value of $\dot{d}(t)$ and the term in brackets is the error.

Returning to Eq. (42) and noting that $\dot{d}$, Δ_0, Δ_1, and θ_2 are uncorrelated variables with zero means, the autocorrelation can be expressed as

$$\phi_v(\tau) = \left[\frac{\omega_0^2}{c^2}\phi_{\dot{d}}(\tau) + \phi_{\Delta_0}(\tau) + \frac{\omega_0^2}{c^2}\phi_{\Delta_1}(\tau) + \phi_{\dot{\theta}_2}(\tau)\right] \qquad (45)$$

and the corresponding power spectral density as

$$\Phi_v(\omega) = \left[\frac{\omega_0^2}{c^2}\Phi_{\dot{d}}(\omega) + \Phi_{\Delta_0}(\omega) + \frac{\omega_0^2}{c^2}\Phi_{\Delta_1}(\omega) + \Phi_{\dot{\theta}_2}(\omega)\right] . \quad (46)$$

Aside from a possible delta function at zero frequency,

$$\Phi_d(\omega) = \frac{1}{\omega^2}\Phi_{\dot{d}}(\omega) \quad (47)$$

and

$$\Phi_{\theta_2}(\omega) = \frac{1}{\omega^2}\Phi_{\dot{\theta}_2}(\omega) . \quad (48)$$

As a result, the power spectral density relation for the receiver structure of Fig. 5 becomes

$$\frac{1}{\omega^2}\Phi_v(\omega) = \Phi_u(\omega) = \frac{1}{\omega^2}\left[\frac{\omega_0^2\omega^2}{c^2}\Phi_d(\omega) + \Phi_{\Delta_0}(\omega) + \frac{\omega_0^2}{c^2}\Phi_{\Delta_1}(\omega) + \omega^2\Phi_{\theta_2}(\omega)\right]$$

or

$$\Phi_u(\omega) = \left[\frac{\omega_0^2}{c^2}\Phi_d(\omega) + \frac{1}{\omega^2}\Phi_{\Delta_0}(\omega) + \frac{\omega_0^2}{c^2\omega^2}\Phi_{\Delta_1}(\omega) + \Phi_{\theta_2}(\omega)\right] . \quad (49)$$

Thus for the two receiver structures, Eqs. (46) and (49) indicate how frequency and Doppler estimation errors and transmitter and receiver phase jitter will affect the measurement of path inhomogeneity effects.

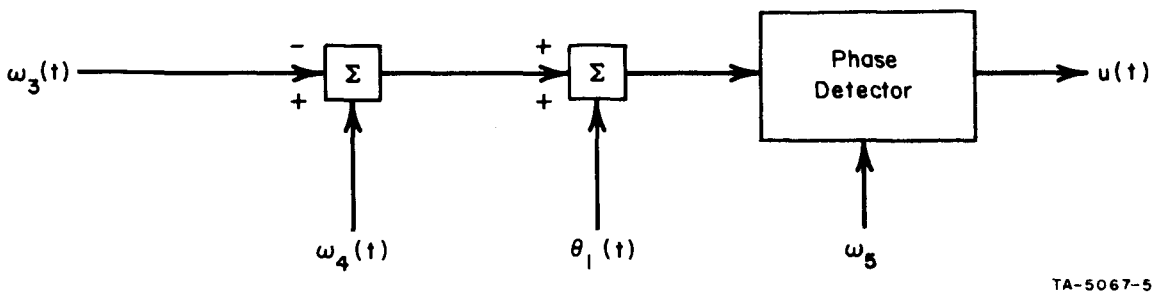

FIG. 5 RECEIVER STRUCTURE (Phase)

2. Measurement of Large Phase Variations

a. INTRODUCTION

Signals in the 1- to 20-Gc frequency band which are propagated through the troposphere may, under severe conditions, experience path-length variations of many wavelengths. When such variations are to be measured electrically, the corresponding phase variations will be many cycles.

Conventional techniques might involve mixing the received signal with a stable reference oscillator at the receiver of the same frequency. Let the received signal be

$$v_1(t) = A \sin [\omega_0 t + \theta(t)] \tag{50}$$

and the local oscillator be

$$v_2(t) = B \cos \omega_0 t \quad . \tag{51}$$

Mixing gives

$$v_3(t) = v_1(t)v_2(t) = \frac{AB}{2} \{\sin [2\omega_0 t + \theta(t)] + \sin \theta(t)\} \tag{52}$$

and low-pass filtering removes the double frequency term giving

$$v_4(t) = \frac{AB}{2} \sin \theta(t) \quad . \tag{53}$$

Since the cosine is a periodic function, such a detector is ambiguous. If we let

$$\phi(t) = \sin^{-1} \frac{2}{AB} v_4(t), \qquad -\frac{\pi}{2} \leq \phi(t) \leq \pi/2 \tag{54}$$

then a particular value of $v_4(t)$ can be produced by a variety of values of $\theta(t)$; *i.e.*,

$$\begin{aligned} \theta(t) &= \phi(t) + 2\pi n \\ \text{or} &= [\pi - \phi(t)] + 2\pi n \end{aligned} \qquad n = \ldots -2, -1, 0, 1, 2 \ldots \tag{55}$$

This ambiguity is not normally important in phase detectors because the phase variation is restricted to the unambiguous region.

Obviously, when phase variations of many cycles are to be detected unambiguously, the conventional detector is inadequate. Four posibilities are described below:

(1) Submultiple voltage-controlled oscillator

(2) Frequency discrimination and integration

(3) Sine-cosine detector

(4) Two-frequency signal.

b. SUBMULTIPLE VOLTAGE—CONTROLLED OSCILLATOR

Suppose that the phase variation is restricted to ±10 cycles and consider the circuit of Fig. 6. Then the angle of Eq. (54),

$$\phi(t) = \sin^{-1} \frac{2}{CD} v(t)$$

is unambiguous in the range $-\pi/2 < \phi(t) < \pi/2$, and further

$$\phi(t) = \frac{\theta(t)}{40} \quad . \tag{56}$$

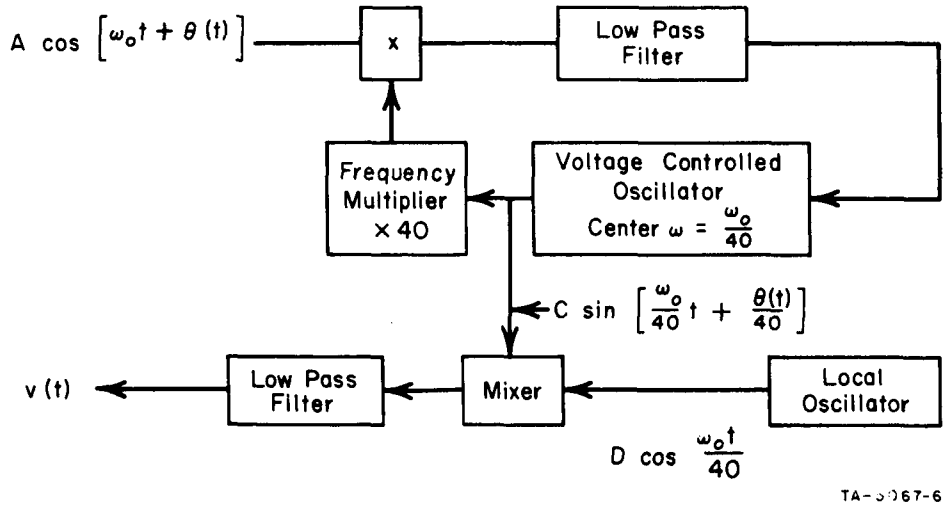

FIG. 6 SUBMULTIPLE VCO PHASE DETECTOR SYSTEM

Therefore, $\theta(t)$ is measured unambiguously in the interval

$$-20\pi < \theta(t) < 20\pi \quad . \tag{57}$$

This technique has the disadvantage of relatively low accuracy, since any error in measurement of $\phi(t)$ is multiplied by 40. However, the submultiple technique could be restricted to the resolution of ambiguities while a tandem conventional phase detector provides accuracy. If other bounds on phase variation are required, the multiplication factor can be changed accordingly.

c. FREQUENCY DISCRIMINATOR AND INTEGRATOR

With the loss of initial phase, which is of no real significance, the incoming signal can be discriminated to obtain a voltage proportional to the instantaneous derivative of phase (frequency). When this voltage is passed through a low-pass filter and integrated, the result is a phase measurement that includes an unknown initial value. No ambiguity exists in this phase measurement. Saturation and stability of integrators are possible problems but not believed to be serious. Integrators with negligible drift over periods of tens of minutes have been built. If saturation is approached, a predetermined increment can be introduced at the integrator input to return the integrator output to its linear region.

Since discriminator noise voltage increases with frequency deviations from the discriminator center frequency, the noise component of the integrator output would be flat with frequency and of approximately the same value it would have in a phase detector output.

d. SINE-COSINE DETECTOR

Suppose the incoming signal of Eq. (1) were mixed with the reference signal of Eq. (51) to give

$$v_4(t) = \frac{AB}{2} \sin \theta(t) \tag{58}$$

and were also mixed with a quadrature reference

$$v_5(t) = B \sin \omega_0 t \quad . \tag{59}$$

The result is

$$v_6(t) = v_1(t)v_5(t) = \frac{AB}{2}[\cos\theta(t) - \cos(2\omega_0 t + \theta(t)] \qquad (60)$$

and low-pass filtering gives

$$v_7(t) = \frac{AB}{2}\cos\theta(t) \quad . \qquad (61)$$

Now ambiguities can be resolved because whenever $v_4(t)$ is near its maximum [when $\theta(t)$ is near $\pi/2$], the sign of $v_7(t)$ will indicate whether $\theta(t)$ is greater or less than $\pi/2$. As $\theta(t)$ varies each time it goes through an odd multiple of $\pi/2$, $v_7(t)$ will change sign. Logic circuitry of moderate complexity will then be required to produce an unambiguous phase output. However, the procedure is straightforward.

Let $\phi(t)$ be defined by Eq. (54) and let

$$\psi(t) = \frac{2}{AB}\cos^{-1} v_7(t) \qquad 0 \le \psi(t) \le \pi \quad . \qquad (62)$$

Define four events as follows:

E_1	$\phi(t) > 0$	$\psi(t)$ changes from + to −
E_2	$\phi(t) < 0$	$\psi(t)$ changes from − to +
E_3	$\phi(t) > 0$	$\psi(t)$ changes from − to +
E_4	$\phi(t) < 0$	$\psi(t)$ changes from + to − .

Let $\theta_b(t)$ be the value of $\theta(t)$ before the event. It is of the form

$$2i\pi + \phi(t)$$

or

$$(2i + 1)\pi - \phi(t) \quad .$$

Let $\theta_a(t)$ be the value of $\theta(t)$ after the event; it is of the same form. For events E_1 or E_2, add π and change the sign of $\phi(t)$; that is,

$$\theta_b(t) = 2i\pi + \phi(t) \rightarrow \theta_a(t) = (2i + 1)\pi - \phi(t)$$

and

$$\theta_b(t) = (2i + 1)\pi - \phi(t) \rightarrow \theta_a(t) = 2(i + 1)\pi + \phi(t) \quad . \qquad (63)$$

Conversely, for events E_3 or E_4, subtract π and change the sign of $\phi(t)$; that is,

$$\theta_b(t) = 2i\pi + \phi(t) \rightarrow \theta_a(t) = (2i - 1)\pi - \phi(t)$$

$$\theta_b(t) = (2i + 1)\pi - \phi(t) \rightarrow \theta_a(t) = 2i\pi + \theta(t) \quad . \tag{64}$$

e. TWO-FREQUENCY SIGNAL

A well-known technique for resolving phase ambiguities is to use two or more phase-coherent tones. To be coherent in phase, two frequencies must be rationally related; *i.e.*, they must both be derived by frequency multiplication of the output of some lower-frequency oscillator. If the two frequencies are

$$\omega_1 = n\omega_0 \tag{65}$$

and

$$\omega_2 = m\omega_0$$

and if the least common multiple of m and n is k, then, assuming no noise, ambiguities over the range of $\pm k$ cycles of ω_0 or $\pm k/n$ cycles of ω_1 can be resolved if perfect phase measurement is possible.

However, in the presence of noise, $m/n(2\pi)$ must be significantly greater than the resulting error in phase measurement. Conversely, in the present problem, the measurement will be meaningless unless the delay variations experienced by the two frequencies in transversing the space-to-earth path are essentially identical. Since the correlation of these variations is a function of the frequency ratio, the ratio m/n should be near unity.

The two requirements of the preceding paragraph are incompatible and the two-frequency technique of phase measurement cannot be used in the proposed experiments.

As an example of the situation, suppose that $\omega_1 = 2\pi 10^9$ radians/sec (1 Gc) and $\omega_2 = 2\pi(1.01)10^9$ radians/sec (1.01 Gc). These two signals differ in frequency by 1 percent and can probably be assumed to have experienced highly correlated phase variations. However, $m/n(2\pi) = 62.8$ milliradians (3.6°). To secure measurements accurate to 62.8 milliradians,

the rms phase jitter should not exceed 20.9 milliradians (3σ level). (For an rms phase jitter of 20.9 milliradians, a signal-to-noise power ratio of 30.6 db is required.) It is very unlikely that such a signal-to-noise ratio can be obtained in a bandwidth sufficiently large to pass the expected phase variations.

f. CONCLUSIONS

Of the four detectors considered, the two-frequency signal technique requires excessive signal-to-noise ratio and the sine-cosine detector is possible but relatively complex. The submultiple voltage-controlled oscillator appears useful if the maximum phase excursion can be bounded in advance and if accuracy is obtained from a separate process.

Only the frequency-discriminator technique appears to present no major difficulties, and is recommended for the proposed experiment.

E. METEOROLOGICAL INSTRUMENTATION

A search of the literature has been made to identify previous experiments and studies from which results and techniques of interest and application to the present investigation might be extracted. A somewhat limited, but nevertheless significant, amount of such information was found to be available from such well-known sources as the National Bureau of Standards, the University of Texas, the Air Force Cambridge Research Laboratories, and the U.S. Navy Electronics Laboratory. These investigations were largely concerned with measurements of the fluctuations of the index of refraction (and related parameters) in the lower troposphere ranging from the microscale (turbulent blobs with dimensions of a few feet) through the mesoscale (cumulus clouds) to the synoptic scale (high and low pressure systems, fronts).

It is now apparent that meteorological observations over all these scales will be required in this experiment. A strictly empirical correlation of synoptic scale observations with bad viewing conditions induced by tropospheric inhomogeneities is likely. Such information is necessary if the results of this experiment are to be readily extrapolated to other meteorological regimes. These observations, though, give no insight into the theoretical understanding of the signal fluctuations. To pinpoint the scale of tropospheric turbulence that will induce detrimental phase fluctuations, the microscale network of observations is required.

Consideration is also being given to the location of the test array. The present concensus is that there are specific advantages to a test site in the south central part of the United States. There the test array would operate at different times in most of the air masses found in the U.S. and would also be exposed to frequent transitions from one air mass to another. The test site should also be chosen as to take advantage of existing upper-air and surface meteorological networks. An especially advantageous site from this standpoint would be an area such as Norman, Oklahoma, where an extensive meteorological instrumentation network is already set up to make mesoscale measurements of severe weather conditions, in connection with the National Severe Storm Project. In such a location, test array operation would require only the additional meteorological instrumentation that is necessary to measure adequately tropospheric variations affecting this particular type of operation.

A study of meteorological instrumentation required at the test site is also under way. Such instruments as ground and airborne refractometers, radio sextants, optical hygrometers and tethered balloons supporting refraction, humidity and temperature sensors are presently under consideration.

Along with the instrumentation outlined above, evaluation of additional remote probing techniques will be carried out. One such possibility which would supply a general indication of the turbulent structure of the troposphere is a sample beyond-the-horizon link whose common volume would be located directly above the test array. (Successful studies relating tropospheric scatter propagation to meteorological factors have been carried out using existing commercial FM transmitters.) The ability of optical radars (lidars) to detect the layer structure of the atmosphere when strong temperature inversions are present has been demonstrated. Further investigation is warranted to determine if such an instrument can be used advantageously in this experiment.

III PROGRAM FOR NEXT REPORTING INTERVAL

Some time will be devoted to suggesting experiments which Goddard Space Flight Center might wish to perform in the near future, and to outlining techniques for arraying the two 85-foot antennas at Fairbanks, Alaska.

Final reports on Project Wideband and on the Triangle Research Institute contract should be received during this next interval and will be reviewed. Other reports from Goddard Space Flight Center, including material on tracking, are expected and will be used where applicable.

The system integration subtask group should complete a preliminary block diagram of the equipment for the proposed experiment.

The signal-source subtask group will continue its investigation of natural sources and nonsatellite platforms and study the effects of satellite orbits. The quality of the measurements of radio-star scintillation at Stanford University will be ascertained, and the possibilities of use of bright-source sunspot radiation will be pursued to determine the state of current knowledge of the brightness, duration, and angular extent of these spots. The uncertainties involved in the use of aircraft and balloon platforms with an interferometer receiving system for estimating magnitude and spectral density of phase fluctuations will be further examined, along with possible methods for reducing these uncertainties. The implications for the satellite-borne transmitter stability and for satellite position-measurement accuracy of using such a receiving system will also be investigated.

The antenna-drive subtask group will seek to answer the following questions:

(1) What are the detailed design equations for the Kalman filter system, assuming motion along both elevation and azimuth axes?

(2) How can information provided by the NASA tracking system be included in this local system to further improve target prediction accuracy?

(3) What are the computational requirements imposed by the Kalman filter system?

(4) If the computational requirements are excessive, what will be the detailed design equations for the nonoptimal system described in Ref. (1)?

(5) What is the performance of the system, *i.e.*, what is the variance of the errors affecting the measurement $\Delta\theta$?

A staff will be assembled for the noise-correlation measurement subtask and will study the required equipment configuration.

The receiver subtask group will seek to choose among the previously examined receiver structures designed to produce measurements of atmosphere-induced amplitude fluctuations, phase fluctuations, and angle-of-arrival fluctuations. It has been concluded that the most useful configuration would employ a four-element "amplitude monopulse" antenna pickup supplying signal to an RF hybrid from which the sum signal and two orthogonal difference signals would be taken. Angle-of-arrival measurements would be obtained by synchronous detection of the difference signals with detector reference supplied either by the hard-limited sum signal or by locking a phase-locked loop to the sum signal. Amplitude fluctuations and phase fluctuations would be measured by demodulation of the sum signal itself. The arguments leading to these conclusions are given in some detail in Ref. (8).

Briefly, the pertinent questions are as follows:

(1) Should the synchronous detection reference be obtained by hard-limiting the sum signal or by locking a phase-locked loop to it?

(2) Should the amplitude fluctuation be measured by envelope detection of the sum signal or by synchronous detection with the phase-locked loop reference?

(3) Should the phase fluctuation be measured by detection with a local reference or by means of a frequency discriminator?

(4) Should the angle-of-arrival measurement be divided by the amplitude measurement (for minimization of the effects of amplitude fluctuations) or should it not?

It is intended to answer these questions by computing the mean-square measurement errors due to noise associated with the various schemes and to look for the receiver structure that yields the lowest rms noise errors. Expressions for the different measurement voltages including noise effects have been derived and have been linearized; the linearization can be justified by the expectation that both the fluctuations of interest

and the noise will be small with respect to total signal strength. By means of these linearized expressions, the noise-induced errors can be identified and their rms values can be computed for different conditions of signal-to-noise ratio, noise spectral shape, etc. It is expected that these calculations will be completed during the third quarter.

A staff will be assembled for the ionospheric measurement subtask and will determine the potential usefulness of various instrumentation, including earth- and satellite-borne sounders.

The meteorological instrumentation subtask group will continue studying the possibilities for test sites, as well as meteorological instrumentation required to support test array operation. Performance of specific instruments will be carefully checked to determine whether such instruments are sensitive enough for the experiment.

IV PRELIMINARY CONCLUSIONS AND RECOMMENDATIONS

Preliminary conclusions at this time are as follows:

(1) The signal platform should be a satellite in a nonequatorial circular orbit with a period of at least 10 hours. This selection will permit observations of reasonable duration at various elevation angles and directions.

(2) Oscillator stability will not limit the accuracy or the range of measurements. Satellite transmitter powers of one watt will give satisfactory signal-to-noise ratios.

(3) The satellite must be compatible with the NASA tracking facilities in order that the experiment can receive angle data for acquisition.

(4) Kalman or similar filtering techniques will be required at the experimental site to provide data for angle-of-arrival and phase measurements.

(5) The satellite should be capable of transmission at frequencies of 2, 4, 8, and 16 Gc in order to cover the frequency range of interest. Since the effects are expected to vary as some power of frequency, a logarithmic distribution of frequencies is recommended. Simultaneous transmission at any two frequencies should permit the separation of tropospheric and ionospheric effects. Provision of coherent sidebands about each carrier will permit the study of phase dispersion in the medium.

(6) Measurement of gain as a function of antenna diameter and analysis of blob size will require a variety of antenna sizes. Diameters of 4, 8, 16, and 32 meters are recommended. These antennas do not need to be moved. For distance-correlation studies, at least one moveable antenna is required, with a diameter of 4 meters. All antennas will require amplitude monopulse feeds and three front ends to cover the required frequency band.

(7) At least two receivers will be required, each having a sum channel, two angle-error channels, and two sideband channels.

REFERENCES

1. J. L. Pawsey and R. N. Bracewell, *Radio Astronomy* (Oxford, The Clarendon Press, 1955).

2. J. Aarons and J. P. Castelli, "Simultaneous Scintillation Observations on 1300-Mc and 3000-Mc Signals Received During the Solar Eclipse of October 2, 1959." *IRE Transactions on Antennas and Propagation,* Volume AP-9 (July 1961).

3. R. S. Allen, J. Aarons, and H. Whitney, "Measurements of Radio Star and Satellite Scintillations at a Subauroral Latitude,' ' *IEEE Transactions on Military Electronics,* Volume MIL-8 (July-October 1964).

4. *Solar-Geophysical Data,* Part B, Published monthly by U.S. Department of Commerce, National Bureau of Standards, Central Radio Propagation Laboratory, Boulder, Colorado.

5. H. A. von Biel, "Tropospheric Phase Fluctuations at S-Band," Technical Documentary Report No. RADC-TDR-63-408, Cornell Aeronautical Laboratory (October 1963).

6. R. B. Battelle, "Feasibility Analysis of a Deep-Space Receiving Terminal Array of Large Equivalent Aperture," Final Report, Contract NAS 1-3075,, Stanford Research Institute, Menlo Park, California (May 1964)(See Appendix 0).

7. R. E. Kalman and R. S. Bucy, "New Results in Linear Filtering and Prediction Theory," *Journal of Basic Engineering*, pp. 95-108 (March 1961).

8. C. H. Dawson, "The Design of an Experiment to Determine the Limitations Imposed on a Multiple-Aperture-Antenna System by Propagation Phenomena," First Quarterly Report, Contract NAS 5-3974, Stanford Research Institute, Menlo Park, California (October 1964).

STANFORD RESEARCH INSTITUTE

MENLO PARK
CALIFORNIA

Regional Offices and Laboratories

Southern California Laboratories
820 Mission Street
South Pasadena, California 91031

Washington Office
808–17th Street, N.W.
Washington, D.C. 20006

New York Office
270 Park Avenue, Room 1770
New York, New York 10017

Detroit Office
1025 East Maple Road
Birmingham, Michigan 48011

European Office
Pelikanstrasse 37
Zurich 1, Switzerland

Japan Office
Nomura Security Building, 6th Floor
1–1 Nihonbashidori, Chuo-ku
Tokyo, Japan

Retained Representatives

Toronto, Ontario, Canada
Cyril A. Ing
67 Yonge Street, Room 710
Toronto 1, Ontario, Canada

Milan, Italy
Lorenzo Franceschini
Via Macedonio Melloni, 49
Milan, Italy